Proc. Estonian Acad. Sci. Phys. Math., 1998, **47**, 1, 29–47
https://doi.org/10.3176/phys.math.1998.1.03

ANALYTIC SOLUTION OF THE STATIONARY ONE-DIMENSIONAL SCHRÖDINGER EQUATION

Matti SELG

Institute of Physics, University of Tartu, Riia 142, EE-2400 Tartu, Estonia; e-mail: matti@fi.tartu.ee

Received 6 October 1997

Abstract. New algorithms are derived and the software composed for fast computing of the one-dimensional wave functions in the range of a continuous energy spectrum. The method can be applied to calculate the quantum-mechanical Franck–Condon factors and the fine structure of the optical spectra of simple quantum systems. This enables us to improve the real potential energy curves of such systems, which is demonstrated for diatomic xenon molecules.

Key words: quantum mechanics, optical spectra, xenon.

1. INTRODUCTION

In this paper a consistently analytic method of solving the one-dimensional stationary Schrödinger equation is described. Its general idea is very simple: the real potential is fitted with several smoothly joined piecewise analytic functions, any component being expressed as a modified Morse potential. The treatment in this paper restricts itself to up to three different Morse-type functions to approximate a potential energy curve (see Section 4.2), but in principle, the method is applicable to an arbitrary number of components. Compared with commonly used numerical methods (see, e.g., [1]), such an analytic approach has several advantages. Firstly, the Schrödinger equation corresponding to a modified Morse potential can always be transformed into a confluent hypergeometric equation that can be easily solved analytically. Secondly, the wave functions for both, discrete and continuous energy spectra, can be easily normalized. Thirdly, very effective and fast algorithms for computing the wave functions can be derived on the basis of the highly developed theory of confluent hypergeometric functions. This circumstance is especially important for complicated fine-structure calculations of the optical spectra, when one has to solve the Schrödinger equation many million

times as fast as possible. Some examples of this kind of computations are given in Section 5 in comparison with relevant experimental data.

In principle, the method can be applied to a wide class of anharmonic potentials. In this paper it is used for diatomic molecules Xe_2, representing a simple but important model system for studying relaxation and radiative decay of excimers. Therefore, to demonstrate the efficacy of the method, we should at first specify the parameters of the potential energy curves for the system under study. In this context it is worth mentioning that the full quantum-mechanical approach described below is especially suitable for the accurate determination of those parameters on the basis of the available experimental data.

2. POTENTIALS FOR THE LOWEST-LYING EXCIMER STATES OF Xe_2*

In view of the spectroscopic applications involved, only the lowest excimer states (0_u^+, 1_u) and the ground state (0_g^+) of Xe_2 are of importance for the study (see Fig. 1). The most important parameters of the lowest dipole allowed excimer state 0_u^+ have been determined in an excellent series of supersonic jet experiments by Stoicheff and co-workers [2]. Unfortunately, the authors tried to fit their data directly to a Morse potential, which was misleading for some later investigations (see [3,4]). As explained elsewhere [5–7], a much better fit can be obtained with the help of a slightly modified Morse potential. Indeed, the data of [2] fitted very well a quadratic function

$$\upsilon_i = T_e + \omega_e\left(n+\frac{1}{2}\right) - \omega_e x_e\left(n+\frac{1}{2}\right)^2, \qquad (1)$$

and adding a cubic term practically did not improve the fit. Consequently, a modified Morse approximation suits well to describe the 0_u^+ state, because (1) would be the exact formula for the vibrational levels of a Morse oscillator

$$V_1(R) = D_1\left(e^{-2\alpha_1(R-R_e)} - 2e^{-\alpha_1(R-R_e)}\right) - A_1, \qquad (2)$$

if one substituted $\omega_e = 2D_1/a$ and $x_e = 1/2a$ with $a = \sqrt{mD_1}/\hbar\alpha_1$. An important point is that the actual dissociation energy D_e = 551.28 meV determined in [2] cannot be identified with the dissociation parameter of a "pure" Morse potential but corresponds to a sum $D_e = D_1 + A_1$. This way, taking D_1 = 515.53 meV, α_1 = 1.91 Å^{-1}, and A_1 = 35.75 meV [5], one gets a very good fit with the data presented in [2].

There still remain some essential problems concerning the potential of the 0_u^+ state. Firstly, one has to fix the equilibrium nuclear separation R_e. As demonstrated elsewhere [8], the best fit with various spectroscopic data can be achieved by taking $R_e = 3.24 \pm 0.01$ Å.

Secondly, one should specify the shape of the potential near its dissociation limit. To solve this problem, let us assume that the approximation (2) holds for all vibrational quantum numbers up to, e.g., $n = 50$. At the point where the level $n = 50$ crosses the Morse potential the latter can be smoothly joined with another curve having a simple analytic form, e.g., that of a "reversed" Morse potential

$$V_2(R) = A_2 - D_2\left(e^{-2\alpha_2(R-R_0)} - 2e^{-\alpha_2(R-R_0)}\right), \qquad (3)$$

with a small hump at long distances. The resulting potential would be nearly the same for different sets of parameters D_2, α_2, and R_0, if one only presumes continuity of the potential and its first derivative. The potential curve presented in the upper part of Fig. 1 has been calculated taking $D_2 = 2.607$ meV, $\alpha_2 = 0.3592$ Å^{-1}, and $R_0 = 10.09$ Å.

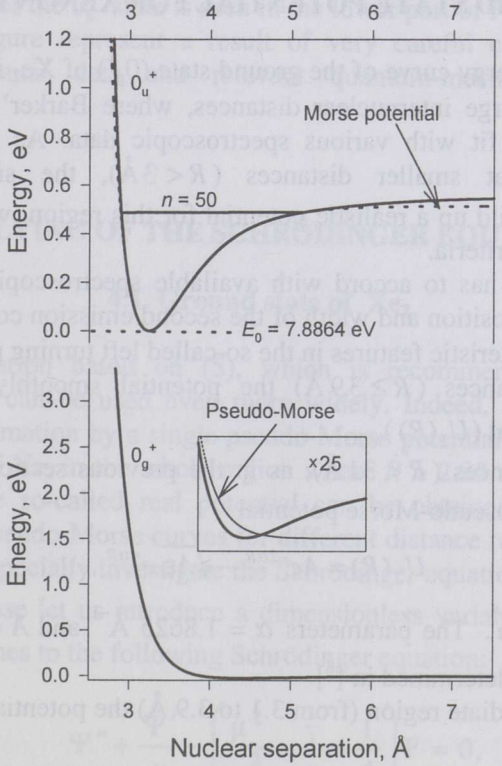

Fig. 1. Potential energy curves for the 0_g^+ and 0_u^+ states of Xe_2. The dashed line in the upper graph corresponds to the "pure" Morse potential. In the insert of the lower graph the region around the shallow (24.3 meV) van der Waals minimum and its pseudo-Morse approximation are demonstrated in a 25 times diminished scale (the curves are almost indistinguishable in the major part of the figure).

Thirdly, in view of the experimental data of Section 5, the approximation (2) obviously cannot be extended to very small internuclear distances. Therefore, it makes sense to use another simple analytic form of the potential

$$V_0(R) = A_0 e^{-2\alpha_0 R} - \sqrt{A_0 \varepsilon_0}\, e^{-\alpha_0 R} - A_3 \qquad (4)$$

for this region. Here, $\varepsilon_0 = \hbar^2 \alpha_0^2 / m$ and $m = 2.4 \times 10^5$ a.u. is the mass of xenon atoms. The potential (4) was smoothly joined with (2) at R = 2.95 Å. The parameters α_0 = 4.66 Å^{-1}, $A_0 = 2.57 \times 10^{11}$ eV, and A_3 = 0.5 eV have been determined in [8].

In this report we have not specially investigated the lowest-lying excimer state 1_u of Xe_2^*. However, for practical purposes the curve obtained for the 0_u^+ state, but shifted down by 0.1–0.15 eV, can be used.

3. GROUND STATE POTENTIAL FOR XENON DIMERS

The potential energy curve of the ground state (0_g^+) of Xe_2 is well determined at comparatively large internuclear distances, where Barker's X_4 potential [9] gives an excellent fit with various spectroscopic data. As regards the steep repulsive region at smaller distances ($R < 3$ Å), the situation is more complicated. To build up a realistic potential for this region, we take account of the following four criteria.

1. The potential has to accord with available spectroscopic data, especially with the observed position and width of the second emission continuum of xenon and with the characteristic features in the so-called left turning point region [3,8].

2. At long distances ($R \geq 3.9$ Å) the potential smoothly transforms into Barker's X_4 potential ($U_1(R)$).

3. At short distances ($R < 3.1$ Å), as in the previous section, the potential is approximated by a pseudo-Morse potential

$$U_2(R) = A e^{-2\alpha R} - \sqrt{A\varepsilon}\, e^{-\alpha R}, \qquad (5)$$

where $\varepsilon = \hbar^2 \alpha^2 / m$. The parameters α = 1.8625 Å^{-1} and $A = 1.1867 \times 10^5$ eV for Xe_2 have been determined in [8].

4. In the intermediate region (from 3.1 to 3.9 Å) the potential is presented as a combination

$$U(R) = (a_0 + a_1 R + a_2 R^2) U_1(R) + (b_0 + b_1 R + b_2 R^2) U_2(R).$$

From demand of continuity of the potential and its first derivative at the boundary points $R_1 = 3.1$ Å and $R_2 = 3.9$ Å, the parameters a_0, a_1, a_2, b_0, b_1, and b_2 can be uniquely determined and the potential therefore fixed.

Criterion 3 probably needs to be commented. Such an approximation for the region of small distances is justified due to its simplicity. On the other hand, the choice of this specific form of the potential is directly related to a simple analytic method used in this paper to solve the Schrödinger equation (see the next section). Another form of (5)

$$U_2(r) = \frac{\varepsilon}{4}(e^{-2\alpha(r-r_0)} - 2e^{-\alpha(r-r_0)}), \quad \text{where} \quad e^{\alpha r_0} = 2\sqrt{A/\varepsilon},$$

more explicitly unveils the physical meaning of the quantities A and ε. Indeed, Morse potential does not have discrete energy spectrum when its well depth $D \le \varepsilon/4$ [10]. Therefore, (5) represents a potential with solely continuous spectrum and this is a justification for the term "pseudo-Morse potential" used to characterize this approximation. Note that ε is a very small quantity ($\varepsilon \approx 0.11$ meV) compared to A and therefore, at small distances the second term in (5) is much smaller than the first one, i.e., the potential is nearly exponential.

The potential for the 0_g^+ state is seen in the lower part of Fig. 1. Both potential curves in this figure represent a result of very careful comparison between various experimental data and relevant quantum-mechanical calculations described in [8].

4. SOLVING OF THE SCHRÖDINGER EQUATION

4.1. Ground state of Xe_2

The approximation based on (5), which is recommended for the short distances' region, can be used even more widely. Indeed, as demonstrated in Fig. 1, the approximation by a single pseudo-Morse potential is quite reasonable for the 0_g^+ state of Xe_2 in the whole region where $R > 2.95$ Å. Naturally, a still better fit with the so-called real potential can be obtained by using several smoothly joined pseudo-Morse curves for different distance regions. In any case, it makes sense to specially investigate the Schrödinger equation corresponding to (5). For this purpose let us introduce a dimensionless variable $y = 2\sqrt{A/\varepsilon}e^{-\alpha R}$. Thereafter one comes to the following Schrödinger equation:

$$\Psi'' + \frac{\Psi'}{y} - \left(\frac{\mu^2}{y^2} - \frac{\frac{1}{2}}{y} + \frac{1}{4}\right)\Psi = 0, \qquad (6)$$

where $\mu = i\sqrt{E/\varepsilon}$ is a pure imaginary parameter determined by the energy (E) of the system. The solution of (6), normalized by the condition

$$\int \Psi_k^* \Psi_{k'} dR = 2\pi\delta(k-k'), \quad k = \sqrt{E/\varepsilon}\,\alpha \tag{7}$$

with right asymptotic behaviour, can be expressed as [10,11]

$$\Psi = e^{-y/2} F(\mu, 2\mu+1, y). \tag{8}$$

Here,

$$F(\mu, 2\mu+1, y) \equiv e^{-i\varphi} y^{\mu} \Phi(\mu, 2\mu+1, y) + e^{i\varphi} y^{-\mu} \Phi(-\mu, -2\mu+1, y), \tag{9}$$

$\Phi(\mu, 2\mu+1, y)$ is the confluent hypergeometric function, and φ is a phase constant (depending on energy) that should be determined from the boundary condition at $R \to 0$.

To calculate the wave functions (8), let us proceed from a very useful Tricomi expansion of the confluent hypergeometric function through the Bessel functions [11,12]:

$$e^{-x/2}\Phi(b, \beta+1, x) = \Gamma(\beta+1)(\kappa x)^{-\alpha/2} \sum_{n=0}^{\infty} A_n\left(\kappa, \frac{1}{2}+\frac{\beta}{2}\right)\left(\frac{x}{4\kappa}\right)^{n/2} \times J_{\beta+n}\left(2\sqrt{\kappa x}\right), \tag{10}$$

where $\Gamma(\beta+1)$ is the gamma-function and $\kappa = \frac{1}{2}+\frac{\beta}{2}-b$. In the case under examination, $b = \mu$, $\beta = 2\mu$, and $\kappa = \frac{1}{2}$. Therefore, after substituting the definition of the Bessel function $J_{2\mu+n}$ into (10), one obtains

$$e^{-x/2}\Phi(\mu, 2\mu+1, x) = \sum_{m,n} \frac{(-1)^m A_n\left(\frac{1}{2}, \mu+\frac{1}{2}\right)}{m!(2\mu+1)_{m+n}} \left(\frac{x}{2}\right)^{m+n}. \tag{11}$$

Here, $(2\mu+1)_m \equiv (2\mu+1)(2\mu+2)\ldots(2\mu+m)$, $A_0 = 1$, $A_1 = 0$, $A_2 = \mu+\frac{1}{2}$, and a recurrent relation holds for the coefficients:

$$nA_n = (n-2)A_{n-2} + 2A_2 A_{n-2} - 2\kappa A_{n-3}, \qquad n = 3, 4, \ldots. \tag{12}$$

Now, let us define the quantities

$$F_k \equiv \frac{A_0}{(2k)!} + \frac{A_2}{(2k-2)!} - \frac{A_3}{(2k-3)!} + \ldots + \frac{A_{2k}}{0!},$$

and prove the following relations:

$$\frac{A_0}{(2k+1)!}+\frac{A_2}{(2k-1)!}-\frac{A_3}{(2k-2)!}+\ldots+\frac{A_{2k}}{1!}-\frac{A_{2k+1}}{0!}=F_k, \tag{13}$$

$$F_k=\frac{\mu+k}{k}\times\frac{\mu+k-1}{k-1}\times\ldots\times\frac{\mu+1}{1}\equiv\frac{(\mu+1)_k}{k!}. \tag{14}$$

The proof can be performed by the mathematical induction method. One can easily check that both assertions are valid for k =1, 2, etc. We now demonstrate that if (13) and (14) hold for some arbitrary k, they also hold for k + 1. Indeed, from (13) we conclude that

$$F_{k+1}(2k+2)=F_k+G_{k+1}, \tag{15}$$

where

$$G_{k+1}\equiv\frac{2A_2}{(2k)!}-\frac{3A_3}{(2k-1)!}+\frac{4A_4}{(2k-2)!}-\ldots-\frac{(2k+1)A_{2k+1}}{1!}+\frac{(2k+2)A_{2k+2}}{0!}.$$

Taking account of (12), one thereafter obtains

$$G_{k+1}=G_k+2A_2F_k+F_{k-1}=2A_2(F_k+F_{k-1}+\ldots+F_0)+(F_{k-1}+F_{k-2}+\ldots+F_0),$$

and thus, according to (15),

$$(k+1)F_{k+1}=(\mu+1)\,(F_k+F_{k-1}+\ldots+F_0)=(\mu+1+k)\,F_k,$$

i.e.,

$$F_{k+1}=\frac{(\mu+1)_{k+1}}{(k+1)!},\ \text{QED.}$$

Substituting (13) and (14) into (11), one comes to the following rapidly converging formula:

$$e^{-x/2}\Phi(\mu,\,2\mu+1,\,x)\equiv C_\mu(x)\,e^{iD_\mu(x)}$$

$$=\sum_{n=0}^{\infty}\frac{F_n}{(2\mu+1)_{2n}}\left(\frac{x}{2}\right)^{2n}\left(1-\frac{x/2}{2\mu+2n+1}\right)=1-\frac{x/4}{\mu+\frac{1}{2}}+\frac{(x/4)^2}{(\mu+\frac{1}{2})1!}\left(1-\frac{x/4}{\mu+\frac{3}{2}}\right)$$

$$+\frac{(x/4)^4}{(\mu+\frac{1}{2})\,(\mu+\frac{3}{2})\,2!}\left(1-\frac{x/4}{\mu+\frac{5}{2}}\right)+\ldots. \tag{16}$$

Using (9) and (16), the wave functions (8) can be easily calculated. A slight problem is, however, how to determine the phase constant φ in (9). To overcome this difficulty, let us express the wave function in the form

$$\Psi = 2C_\mu \cos(D_\mu + \varphi_0 - kR), \tag{17}$$

where the functions C_μ and D_μ are defined in (16), $k=\sqrt{E/\varepsilon}\,\alpha$ and $\varphi_0=\sqrt{E/\varepsilon}\,\ln(2\sqrt{A/\varepsilon}\,)-\varphi$. As is known (see, e.g., [11]), the modulus of the confluent hypergeometric function exponentially increases in the range of small internuclear disctances. At the same time the wave function should rapidly disappear in the classically forbidden region. Consequently, $\cos(D_\mu+\varphi_0-kR)\approx 0$ at any distance $R << R_0$, where R_0 is determined by the condition $U(R_0)=E$. This gives ground to a very simple and precise method of calculating the phase constant φ_0. One only has to evaluate the function (15) at a suitable point $X_0<< R_0$. Thereafter, φ_0 is determined from the condition

$$\tan\varphi_0 = \cot(D_\mu(X_0) - kX_0). \tag{18}$$

In this context it should be pointed, however, that a high computer precision is needed for the accurate calculation of the phase constant according to (18). An example of a ground state wave function, calculated as described in this section, is seen in Fig. 2.

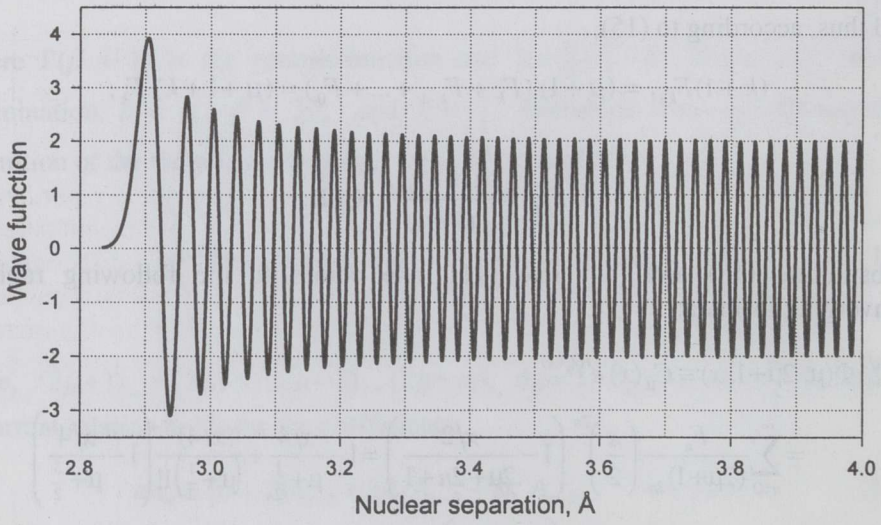

Fig. 2. A ground state wave function of Xe_2 corresponding to the pseudo-Morse potential (5) at energy $E = 2.5$ eV.

4.2. 0_u^+ state of the excimer Xe_2^*

In this section we presume that energy is measured relative to the potential's minimum. We do not examine specially the highest bound states in the narrow energy range $D_1 < E < D = D_1 + A_1$ (see Section 2), not so important for spectroscopic applications. Therefore, when studying the bound states of xenon excimers in the 0_u^+ state, we restrict ourselves to the vibrational levels $n \leq 50$, when description in terms of the "pure" Morse potential (2) is applicable. The wave functions in this case can be calculated in a standard manner. However, for the wave functions of upper vibrational levels an effective algorithm that enables simultaneous determination of all zeros of the confluent hypergeometric function could be used [5].

Let us consider now the continuum states $E \geq D$. Examination of this energy region is important, e.g., for the adequate interpretation of the observed emission corresponding to the classical left turning points of free Xe*–Xe pairs. This way one gets very useful information on the potential energy curves at very small distances (down to about 2.7 Å [8]). According to Section 2, three different but smoothly joined distance regions of the potential curve should be studied: 1. $R < 2.95$ Å, 2. 2.95 Å $\leq R \leq$ 5.09 Å (the point where the level $n = 50$ crosses the potential curve), and 3. $R > 5.09$ Å.

A pseudo-Morse approximation (4), very similar to that described in the previous section, is used for region 1, a "reversed" Morse potential (3) is adjusted for region 3, and the Morse potential (2) is applied to the bound states' region 2. One has to solve the Schrödinger equation for each of these areas and merge the separated parts requiring, as usual, continuity of the wave function and its first derivative (or logarithmic derivative) at the boundary points (2.95 Å and 5.09 Å). Compared with earlier reports [5–7], essentially improved algorithms regarding regions 2 and 3 are presented here. Another new element is special account taken of the small distances' area 1. Let us, therefore, begin with studying the wave functions corresponding to region 1. The treatment is completely analogous to that in the previous section. Thus, if energy is measured relative to the minimum of the potential well and if one takes account of the differences of the parameters in (4) and (5), the wave function can be expressed as

$$\Psi = C_1 C_\mu^{(1)} \cos(D_\mu^{(1)} + \varphi_0^{(1)} - k_1 R), \qquad (17')$$

where $C_\mu^{(1)}$ and $D_\mu^{(1)}$ are given by (16), $\varphi_0^{(1)}$ can be determined from (18), $\mu = i\sqrt{(E-D)/\varepsilon_0}$, and $k_1 = \mu\alpha_0$. The main difference from the previous case is that one cannot fix the normalization factor C_1, because (17′) cannot be extended to the free particle's region. The superscript is introduced to distinguish the symbols here from the ones in the previous section. We also have to evaluate the derivative (or logarithmic derivative) of (17′) in the boundary point

$R_0^{(1)} = 2.95$ Å. The procedure is analogous to that described in [6]. As a result, the following formula is obtained:

$$F_1 \equiv \frac{\Psi'}{\Psi} = \frac{\alpha_0 y}{2} + k_1 \frac{C_{\mu+1}^{(1)}}{C_\mu^{(1)}} \frac{\sin(D_{\mu+1}^{(1)} + \varphi_0^{(1)} - k_1 R)}{\cos(D_\mu^{(1)} + \varphi_0^{(1)} - k_1 R)}, \tag{19}$$

where $C_{\mu+1}^{(1)}(x)\, e^{iD_{\mu+1}^{(1)}(x)} \equiv e^{-x/2}\Phi(\mu+1,\, 2\mu+1,\, x)$. From a general formula for confluent hypergeometric functions [11]

$$\Phi(\mu+1,\, 2\mu+1,\, x) = e^{x}\Phi(\mu,\, 2\mu+1,\, -x)\,,$$

i.e.,

$$e^{-x/2}\Phi(\mu+1,\, 2\mu+1,\, x) = e^{x/2}\Phi(\mu,\, 2\mu+1,\, -x), \tag{20}$$

we see that the functions $C_{\mu+1}^{(1)}$ and $D_{\mu+1}^{(1)}$ can also be calculated with the help of (16), if one only substitutes the negative argument $x = -y = -2\sqrt{A_0/\varepsilon_0}\; e^{-\alpha_0 R_0}$ into this formula.

Now, let us examine region 2 (still assuming $E \geq D$), where the wave function is expressed by

$$\Psi = e^{-y/2} F(-\gamma,\, 2\mu+1,\, y). \tag{21}$$

Here,

$$F(-\gamma,\, 2\mu+1,\, y) \equiv e^{-i\varphi} y^{\mu}\, \Phi(-\gamma,\, 2\mu+1,\, y) + e^{i\varphi} y^{-\mu}\, \Phi(-\gamma^*,\, -2\mu+1,\, y), \tag{22}$$

$y = 2ae^{-\alpha_1 R}$, $\mu = ia\sqrt{(E - D_1)/D_1}$, and $\gamma = a - \mu - \frac{1}{2}$ (see (2) for other definitions). Again, we can use the Tricomi expansion (10) and the recurrent relation (12) to simplify the calculation of confluent hypergeometric functions in (22). In this case, $b = -\gamma$, $\beta = 2\mu$, and $\kappa = a$. As a result of a deduction like that leading to (16), one comes to the following main formula for region 2:

$$e^{-x/2}\Phi(-\gamma,\, 2\mu+1,\, x) \equiv C_\mu^{(2)}(x)\, e^{iD_\mu^{(2)}(x)} = \sum_{n=0}^{\infty} B_n, \tag{23}$$

where $B_0 = 1$, $B_1 = -\dfrac{ay}{2\mu+1}$, and

$$B_n = \frac{y}{n(2\mu+n)}\left(-aB_{n-1} + \frac{y}{4}B_{n-2}\right), \quad n = 2, 3, \ldots . \tag{24}$$

Formulae (23) and (24) can also be applied to calculate another function $e^{-x/2}\Phi(-\gamma+1, 2\mu+1, x)$ that is needed to evaluate the derivatives of the wave function at the boundary points. For this purpose we only should replace $a \to a-1$. Thus, defining the function $C^{(2)}_{\mu+1}(x)\, e^{iD^{(2)}_{\mu+1}(x)} \equiv e^{-x/2}\Phi(-\gamma+1, 2\mu+1, x)$, one easily obtains

$$F_2 \equiv \frac{\Psi'}{\Psi} = \alpha_1\left(\frac{y+1}{2} - a\right) + k_2 \frac{C^{(2)}_{\mu+1}}{C^{(2)}_{\mu}} \frac{\sin(D^{(2)}_{\mu+1} + \varphi^{(2)}_0 - k_2 R)}{\cos(D^{(2)}_{\mu} + \varphi^{(2)}_0 - k_2 R)},$$

$$\alpha_1\left(a - \frac{1}{2}\right)\frac{C^{(2)}_{\mu+1}}{C^{(2)}_{\mu}} \frac{\cos(D^{(2)}_{\mu+1} + \varphi^{(2)}_0 - k_2 R)}{\cos(D^{(2)}_{\mu} + \varphi^{(2)}_0 - k_2 R)}. \qquad (25)$$

On the basis of Eqs. (21)–(25) the wave function in region 2 can be written as

$$\Psi = C_2 C^{(2)}_{\mu} \cos(D^{(2)}_{\mu} + \varphi^{(2)}_0 - k_2 R), \qquad (17'')$$

where $k_2 = \alpha\mu$ and the phase constant $\varphi^{(2)}_0$ is determined from the equation

$$F_1(R^{(1)}_0) = F_2(R^{(1)}_0), \; (R^{(1)}_0 = 2.95 \text{ Å}) \qquad (26)$$

according to (19) and (25). The normalization factor C_2 will be fixed later.

The treatment of distance range 3 based on the "reversed" Morse potential (3) is analogous to that of region 2. The same basic formulae (21)–(26) can be used if one makes the following adjustments of the parameters:

$$a \to ia_2 \equiv i\sqrt{mD_2}/\hbar\alpha_2, \; y \to iy_2 \equiv 2ia_2\, e^{-\alpha_2 R},$$

$$\text{and } \mu \to i\mu \equiv ia_2\sqrt{(E - D + D_2)/D_2}$$

(note that μ is a real quantity here, because $E \geq D$). As a result, the wave function in this region becomes (see [6] for details)

$$\Psi = 2C^{(3)}_{\mu} \cos(D^{(3)}_{\mu} + \varphi^{(3)}_0 - k_3 R), \qquad (17''')$$

where $k_3 = \alpha_2\mu$,

$$C^{(3)}_{\mu}(y_2) e^{iD^{(3)}_{\mu}(y_2)} \equiv e^{-iy_2/2}\Phi\left(-i(a_2 - \mu) + \frac{1}{2}, 2i\mu + 1, iy_2\right) = \sum_{n=0}^{\infty} B_n, \qquad (27)$$

with $B_0 = 1$, $B_1 = \dfrac{a_2 y}{2i\mu + 1}$, and

$$B_n = \frac{y}{n(2i\mu + n)}\left(a_2 B_{n-1} - \frac{y}{4} B_{n-2}\right), \quad n = 2, 3, \ldots. \qquad (28)$$

At large distances, as needed, (17''') approaches the free wave form. To calculate the logarithmic derivative in region 3, another function

$$C_{\mu+1}^{(3)}(x)e^{iD_{\mu+1}^{(3)}(x)} \equiv e^{-iy_2/2}\Phi\left(-i(a_2-\mu)+\frac{3}{2},\ 2i\mu+1,\ iy_2\right)$$

is needed. Similarly to the previous cases, it can be evaluated with the help of the same main formulae (27) and (28) if one replaces $a_2 \to a_2 + i$. The logarithmic derivative in region 3 then becomes

$$F_3 \equiv \frac{\Psi'}{\Psi} = k_3 - \alpha_2 \frac{y-1}{2} + (\alpha_2 a_2 - k_3)\tan(D_\mu^{(3)} + \varphi_0^{(3)} - k_3 R)$$

$$- \frac{C_{\mu+1}^{(3)}}{C_\mu^{(3)}}\left(\frac{\alpha_2/2\cdot\cos\left(D_{\mu+1}^{(3)} + \varphi_0^{(3)} - k_3 R\right) + (\alpha_2 a_2 - k_3)\sin\left(D_{\mu+1}^{(3)} + \varphi_0^{(3)} - k_3 R\right)}{\cos(D_\mu^{(3)} + \varphi_0^{(3)} - k_3 R)}\right), \tag{29}$$

and the phase constant $\varphi_0^{(3)}$ is determined from the boundary condition

$$F_2(R_0^{(2)}) = F_3(R_0^{(2)}),\ (R_0^{(2)} = 5.09\ \text{Å}). \tag{30}$$

Thus, we have fixed the phase constants in three different distance regions under examination. From demand of continuity of the wave functions (17′), (17″), and (17‴) at the boundary points $R_0^{(1)}$ and $R_0^{(2)}$, we can now easily determine the normalization factors C_1 and C_2. Therefore, we have completed all the procedures needed for fast analytic solving of the Schrödinger equation corresponding to the 0_u^+ state of Xe_2^*. In Fig. 3, three characteristic wave functions, calculated at essentially different energy values, are presented.

5. QUANTUM-MECHANICAL FRANCK–CONDON FACTORS FOR THE ELECTRONIC TRANSITION $0_u^+ \to 0_g^+$ IN Xe_2

In this paper we do not examine the variation of the molecular transition moment with internuclear separation, assuming therefore that it does not change dramatically within the range of interest for Xe_2 [13]. Therefore, in examples presented below the emission profiles are calculated simply by summing the relevant integrated Franck–Condon factors. The common (semiclassical) method of calculating these factors for any fixed vibrational level n is based on the well-known formula

$$W_n(E_0) \propto E_0^3 \left|\Psi_n(R)\right|^2 \Big/ \left|\frac{dU(R)}{dR}\right|, \tag{31}$$

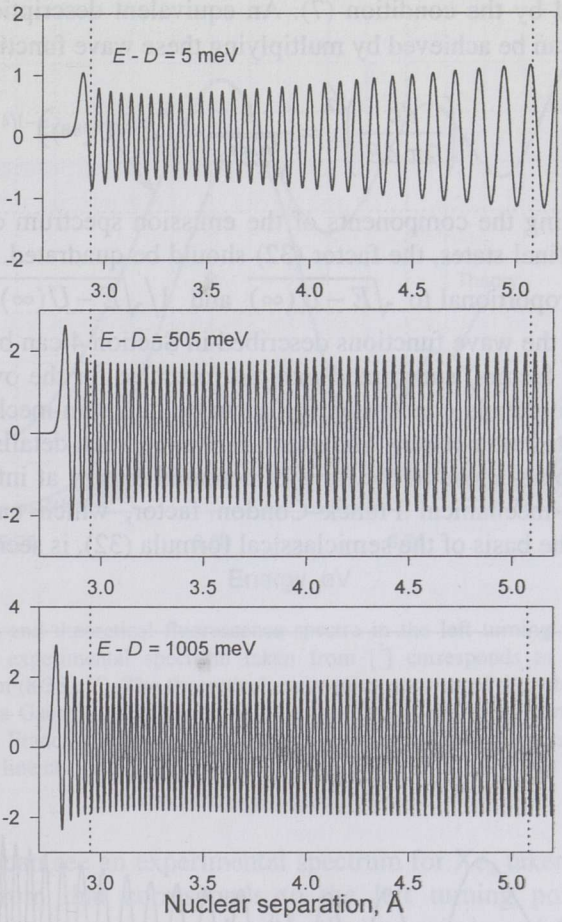

Fig. 3. Wave functions for the 0_u^+ state of the excimer Xe_2^* calculated at energies 5, 505, and 1005 meV above the dissociation limit. The dashed vertical lines correspond to the boundary points $R_0^{(1)} = 2.95$ Å and $R_0^{(2)} = 5.09$ Å that separate three differently treated parts of the wave functions.

where $W_n(E_0)$ is the Franck–Condon factor, $\Psi_n(R)$ is the wave function of the vibrational state n, and $U(R) \equiv U_1(R) - U_2(R) = E_0$ is the difference between the upper (U_1) and lower (U_2) potentials.

Our treatment is completely quantum-mechanical. On the other hand, we do not restrict ourselves to studying only the bound-free transitions. Consequently, there is no need to use the simplified formula (31) that describes quantum-mechanically only the initial bound state and does not account correctly for changing the density of final states (proportional to $\sqrt{E - U(\infty)}$; [14]), especially at small energies. The wave functions corresponding to the continuous spectrum

are normalized by the condition (7). An equivalent description in terms of the energy space can be achieved by multiplying these wave functions with [10]

$$\left(\frac{dk}{2\pi\, dE}\right)^{1/2} = \frac{1}{\sqrt{2\pi\hbar v}} \propto \left(E - U(\infty)\right)^{-1/4}. \tag{32}$$

When calculating the components of the emission spectrum corresponding to a continuum of final states, the factor (32) should be quadrated. Consequently, the two factors, proportional to $\sqrt{E-U(\infty)}$ and $1/\sqrt{E-U(\infty)}$, respectively, are cancelled, and the wave functions described in Section 4 can be directly (without any additional factors) substituted into the formulae for the overlap integrals. In many cases the details concerning the accurate quantum-mechanical description of the final states are not very important. However, such details become crucial if total energy comes close to the limit of potential energy at infinity. An example of a quantum-mechanical Franck–Condon factor, which cannot be correctly computed on the basis of the semiclassical formula (32), is seen in Fig. 4.

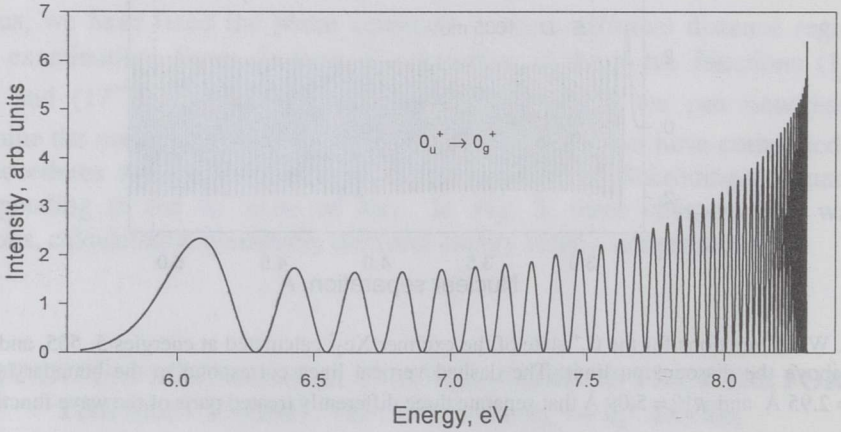

Fig. 4. An integrated Franck–Condon factor corresponding to the vibrational level $n = 40$ of the 0_u^+ state of the excimer Xe_2^*.

6. COMPARISON BETWEEN THEORY AND EXPERIMENT

6.1. Oscillatory structures in bound-free fluorescence spectra of Xe_2 corresponding to the left turning point region of Xe_2^*

Time-resolved fluorescence measurements related to the inner part of the excimer states provide useful information for checking potential curves at small distances. As unambiguously demonstrated by Möller et al. [3], such an emission originates from the left turning points of the bound excimers.

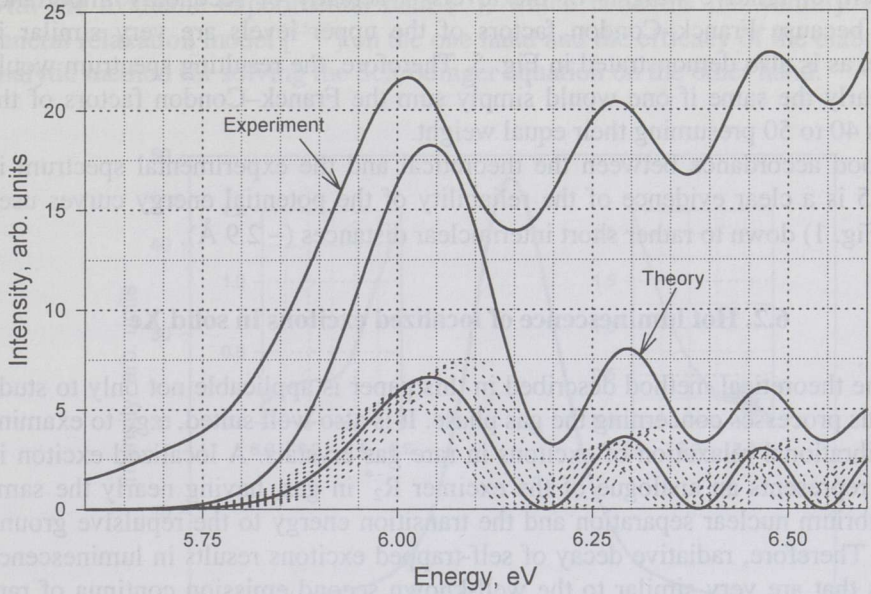

Fig. 5. Experimental and theoretical fluorescence spectra in the left turning point region of the excimer Xe_2^*. The experimental spectrum taken from [3] corresponds to a selective optical excitation of 148 nm (8.38 eV). The theoretical curve takes account of the vibrational levels from 30 to 50, assuming a Gaussian distribution of their weights. In the lower part of the figure (in a different scale) the Franck–Condon factors of the levels n = 36–44 (from right to left) are presented. The solid line corresponds to $n = 40$.

In Fig. 5 one can see an experimental spectrum for Xe_2 taken from [3], and a calculated spectrum that corresponds to the left turning point region. The experimental spectrum was recorded within the time window of 4 ns immediately after the exciting spectrally selected synchrotron radiation pulse. At room temperature the excitation wavelength for the curve presented in Fig. 5 (148 nm) suits best to populate the vibrational levels n = 45–50 of xenon excimers in the 0_u^+ state. Therefore, due to possible slight relaxation during registration, it seems reasonable to presume a Gaussian distribution of relative statistical weights of the levels that contribute to the emission in the left turning point region:

$$g_n \propto e^{-\left(\frac{n-n_0}{\Delta n}\right)^2}. \qquad (33)$$

This simple model was used to fit the experimental spectrum to the relevant theoretical one. Quantum-mechanical Franck–Condon factors for the vibrational levels 30 to 50 of the 0_u^+ state were calculated and summed according to (33), taking $n_0 = 40$ and $\Delta n = 5$. A pseudo-Morse approximation was used for the repulsive ground state and the calculations involved continuum states in the range from 0.5 to 3.0 eV. The result is seen in Fig. 5. Note, however, that the

problem of relative weights of the levels is actually of secondary importance here, because Franck–Condon factors of the upper levels are very similar in shape, as is also demonstrated in Fig. 5. Therefore, the resulting spectrum would be nearly the same if one would simply sum the Franck–Condon factors of the levels 40 to 50 presuming their equal weight.

Good accordance between the theoretical and the experimental spectrum in Fig. 5 is a clear evidence of the reliability of the potential energy curves used (see Fig. 1) down to rather short internuclear distances (~ 2.9 Å).

6.2. Hot luminescence of localized excitons in solid Xe

The theoretical method described in this paper is applicable not only to study various processes concerning the gas phase. It is also well suited, e.g., to examine the vibrational relaxation of excitons in rare gas crystals. A localized exciton in solid represents an analogue of the excimer R_2^* in gas, having nearly the same equilibrium nuclear separation and the transition energy to the repulsive ground state. Therefore, radiative decay of self-trapped excitons results in luminescence bands that are very similar to the well-known second emission continua of rare gases (see, e.g., [4]).

Recently a nonperturbational theory of multiphonon anharmonic decay of strongly excited local modes in crystals was worked out [15,16]. Here this new theoretical model is applied to describe the two-phonon anharmonic decay of vibrationally strongly excited quasimolecular emission centres Xe_2^* in solid xenon. The same potential curves described in Sections 2 and 3 are used, and the treatment concerns only the bound states' region 2 (see Section 4.2) of the upper electronic state. As regards the ground state potential, this is just the case when a single pseudo-Morse approximation can be successfully used for all internuclear distances (roughly from 3 to 4 Å).

The peculiarities of the vibrational relaxation of the system under study are described in detail elsewhere [17]. The most important point is that sharp acceleration of the two-phonon decay rate is expected for the quasimolecule Xe_2^* near a critical vibrational level ($n_{cr} = 23$) and such relaxation jumps should reveal themselves in the hot luminescence spectrum of solid xenon. To verify these theoretical predictions, one has to calculate all Franck–Condon factors for the levels n = 0–44 (see an example in Fig. 4), ascertain their relative statistical weights by solving the corresponding system of kinetic equations, and finally sum them up to obtain the desired hot luminescence spectrum. It should be pointed out that fully quantum-mechanical calculation of the Franck–Condon factors is absolutely needful to get the correct hot luminescence spectrum (containing the oscillatory structures on the high-energy side) of the quasimolecule Xe_2^*. Indeed, as has been checked, semiclassical approaches like (31) lead to completely wrong emission profiles in this case. The resulting spectrum presented in Fig. 6 also contains a contribution from the zeroth level of the 1_u state. The calculated hot luminescence spectrum is in good accordance

with the available experimental data [18], which confirms the validity of the general relaxation model [15,16] on the one hand and the efficacy of the elaborated analytic method for solving the Schrödinger equation on the other hand.

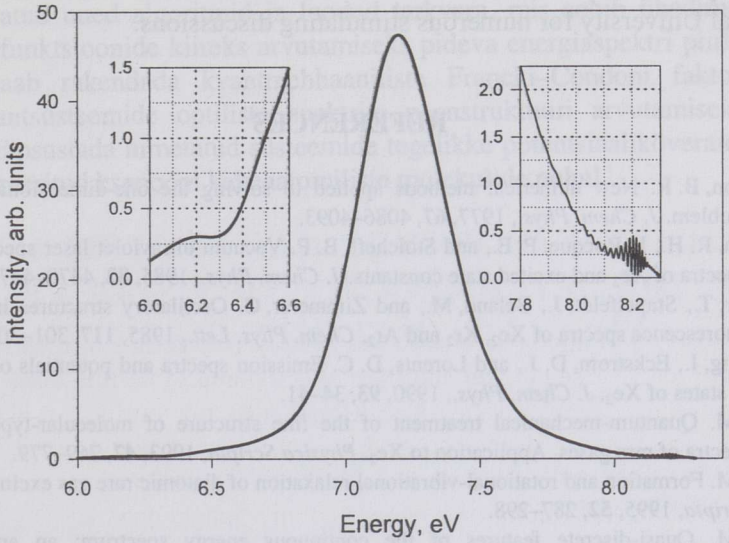

Fig. 6. Calculated hot luminescence spectrum of the quasimolecule Xe_2^* in solid Xe. The characteristic features depicted in the inserts cannot be explained by the common perturbation theory.

7. CONCLUSIONS

The main goal of this paper was to demonstrate that the consistently analytic method of solving the Schrödinger equation is well suited to spectroscopic study of simple one-dimensional quantum systems. The author has composed a set of 32-bit computer programs based on the algorithms described in Section 4. This special software was the main tool that enabled the quantum-mechanical calculations briefly described in Section 6 (much more examples are presented in [8]), and fixing the parameters of the potential energy curves given in Sections 2 and 3. It is worth mentioning that, compared with the previous ones [5–7], these new algorithms ensure a win in the computation speed of at least ten times, simultaneously essentially reducing the demands for the precision of the calculations. Therefore, it is expected that the elaborated method will be used much more widely than for solely studying diatomic rare gas molecules (or quasimolecules).

ACKNOWLEDGEMENTS

The work was supported by grants Nos. 352 and 2689 from the Estonian Science Foundation. The author is grateful to Prof. V. Hizhnyakov from the University of Tartu as well as to Dr. A. Ulrich and Dr. J. Wieser from Munich Technical University for numerous stimulating discussions.

REFERENCES

1. Johnson, B. R. New numerical methods applied to solving the one-dimensional eigenvalue problem. *J. Chem. Phys.*, 1977, **67**, 4086–4093.
2. Lipson, R. H., LaRocque, P. E., and Stoicheff, B. P. Vacuum ultraviolet laser spectroscopy. II. Spectra of Xe_2 and excited state constants. *J. Chem. Phys.*, 1985, **82**, 4470–4478.
3. Möller, T., Stapelfeldt, J., Beland, M., and Zimmerer, G. Oscillatory structures in bound-free fluorescence spectra of Xe_2, Kr_2 and Ar_2. *Chem. Phys. Lett.*, 1985, **117**, 301–306.
4. Messing, I., Eckstrom, D. J., and Lorents, D. C. Emission spectra and potentials of the 0_u^+ and 1_u states of Xe_2. *J. Chem. Phys.*, 1990, **93**, 34–41.
5. Selg, M. Quantum-mechanical treatment of the fine structure of molecular-type absorption spectra of rare gases. Application to Xe_2. *Physica Scripta*, 1993, **47**, 769–779.
6. Selg, M. Formation and rotational-vibrational relaxation of diatomic rare gas excimers. *Physica Scripta*, 1995, **52**, 287–298.
7. Selg, M. Quasi-discrete features of the continuous energy spectrum: an application to metastable Xe*–Xe pairs. *J. Phys. B: At. Mol. Opt. Phys.*, 1996, **29**, 699–713.
8. Selg, M., Ulrich, A., Wieser, J., Murnick, D. E., and Kisand, V. Emission from the left turning point region of the rare gas excimers. *J. Chem. Phys.* (in press).
9. Barker, J. A. Second virial coefficients and interatomic potentials for inert gases. *J. Chem. Phys.*, 1975, **63**, 2767–2768.
10. Landau, L. D. and Lifshits, E. M. *Kvantovaya mekhanika. Nerelyativistskaya teoriya.* Nauka, Moscow, 1989 (in Russian).
11. Bateman, H. and Erdélyi, A. *Higher Transcendental Functions. Vol. 1.* McGraw-Hill, New York, 1953.
12. Tricomi, F. *Ann. Mat. Pura Appl.*, 1949, **28**, 263–290.
13. Castex, M.-C. Experimental determination of the lowest excited Xe_2 molecular states from VUV absorption spectra. *J. Chem. Phys.*, 1981, **74**, 759–771.
14. Levitch, V. G. *Kurs teoreticheskoj fiziki. Vol. 1.* Fizmatgiz, Moscow, 1962 (in Russian).
15. Hizhnyakov, V. Relaxation jump of strong vibration. *Phys. Rev. B*, 1996, **53**, 13 981–13 984.
16. Hizhnyakov, V. and Nevedrov, D. Stepwise quantum decay of self-trapped solitons. *Phys. Rev B*, 1997, **56**, R2908–R2911.
17. Hizhnyakov, V. and Selg, M. Relaxation jumps and hot luminescence of self-trapped excitons. *J. Luminesc.* (in press).
18. Kink, R., Lõhmus, A., and Selg, M. Self-trapping and hot luminescence of excitons in rare gas solids. *Phys. Status Solidi B*, 1981, **107**, 479–490.

ÜHEDIMENSIOONILISE STATSIONAARSE SCHRÖDINGERI VÕRRANDI ANALÜÜTILINE LAHENDAMINE

Matti SELG

On tuletatud uued algoritmid ja loodud tarkvara, mis sobib ühedimensioonilise lainefunktsioonide kiireks arvutamiseks pideva energiaspektri piirkonnas. Meetodit saab rakendada kvantmehhaaniliste Francki–Condoni faktorite ja lihtsate kvantsüsteemide optiliste spektrite peenstruktuuri arvutamiseks. See võimaldab täpsustada nimetatud süsteemide tegelikke potentsiaalikõveraid, mida on demonstreeritud ksenooni kaheaatomiliste molekulide puhul.